Supporting Information

Exploring the structural conditions favoring Au anionic behavior on Au doped CeO_2.

L. E. López-González[*1], R. Ponce-Pérez, Sergio A. Aguila, Mario H. Farías, T. A. Zepeda-Partida, F. F. Castillon-Barraza, J. Guerrero-Sanchez[*1]

[1]*Centro de Nanociencias y Nanotecnología, Universidad Nacional Autónoma de México, Ensenada, BC 22860, Mex.*

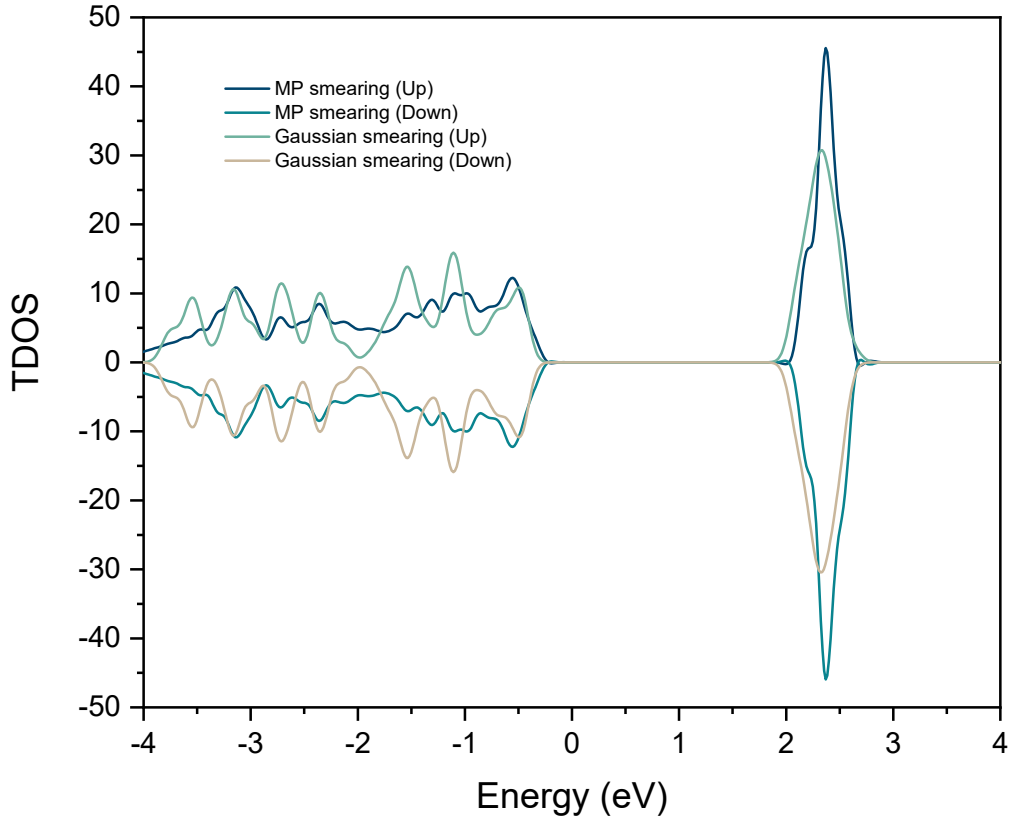

Figure S1. Total density of states (TDOS) for bulk CeO_2, comparing Gaussian and Methfessel-Paxton smearing

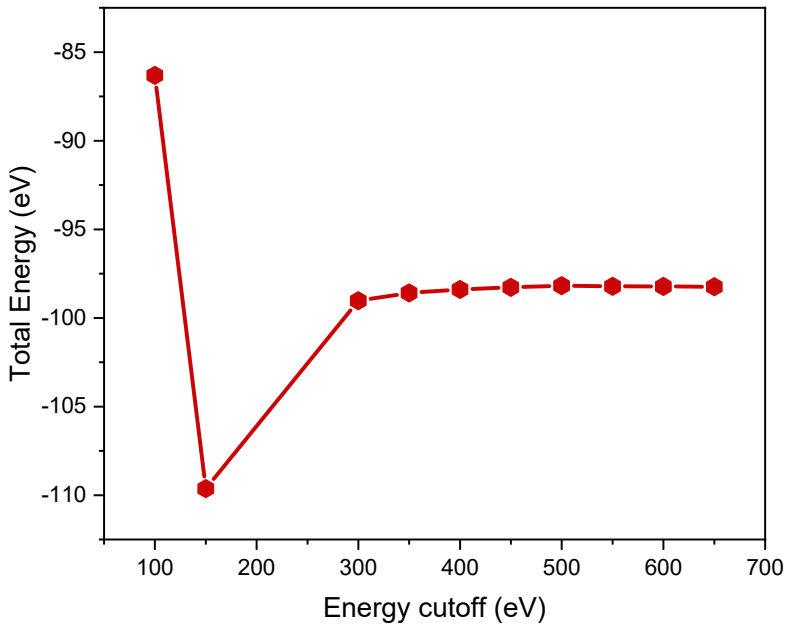

Figure S2. Energy cutoff as a function of total energy for the bulk parametrization of CeO_2 model.

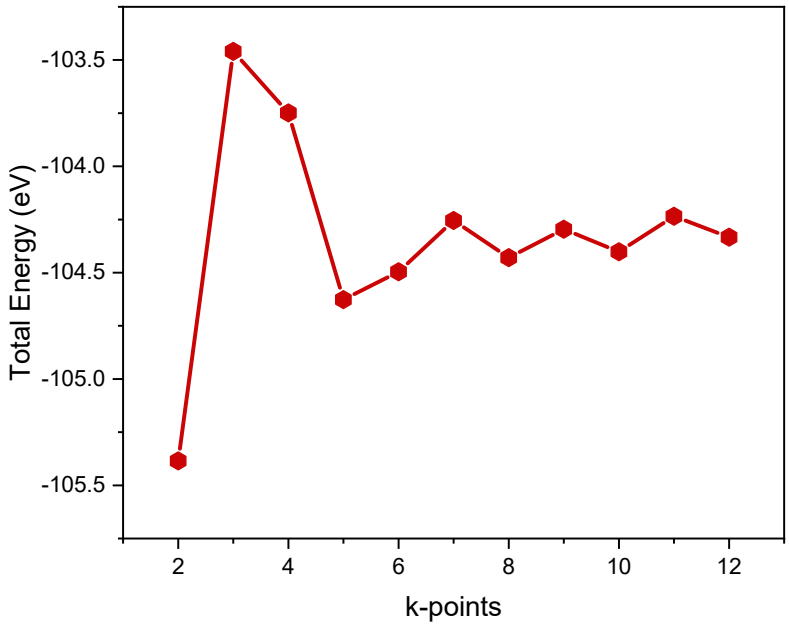

Figure S3. K-point mesh as a function of total energy for the bulk parametrization of CeO_2 model.

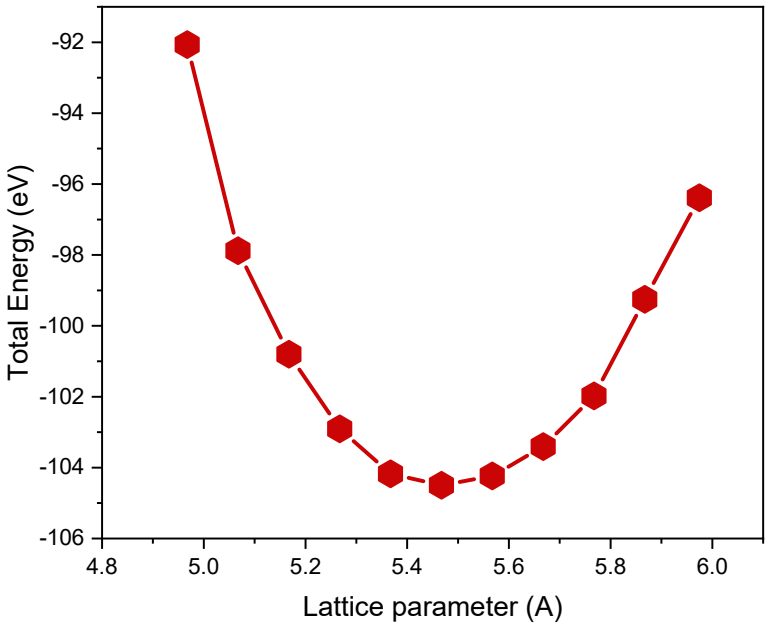

Figure S4. Lattice parameter as a function of total energy for the bulk parametrization of CeO_2 model.

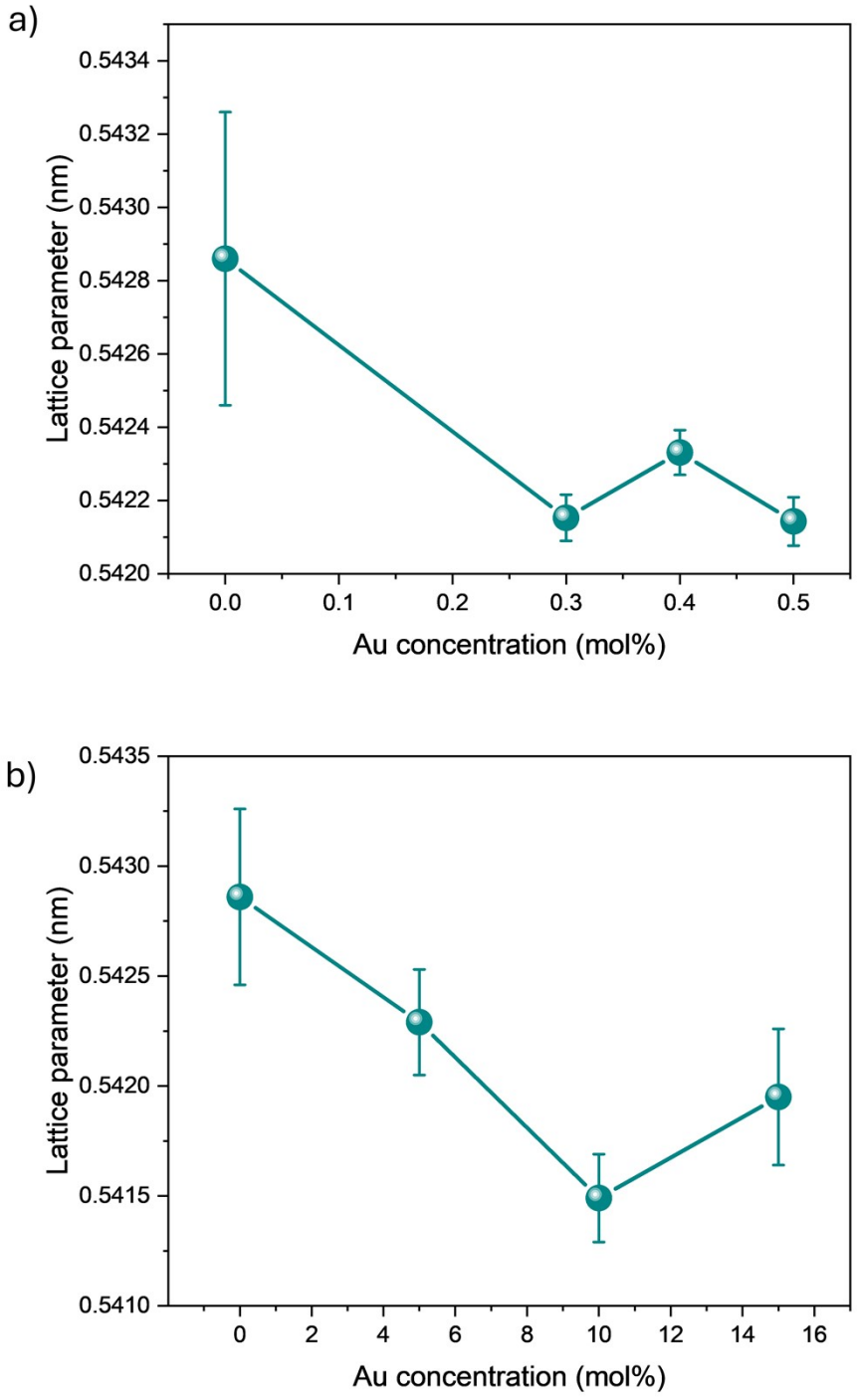

Figure S5. X-ray diffraction determination of the lattice parameter as a function of gold concentration for (a) Low Au concentration and (b) high Au concentration regimes.

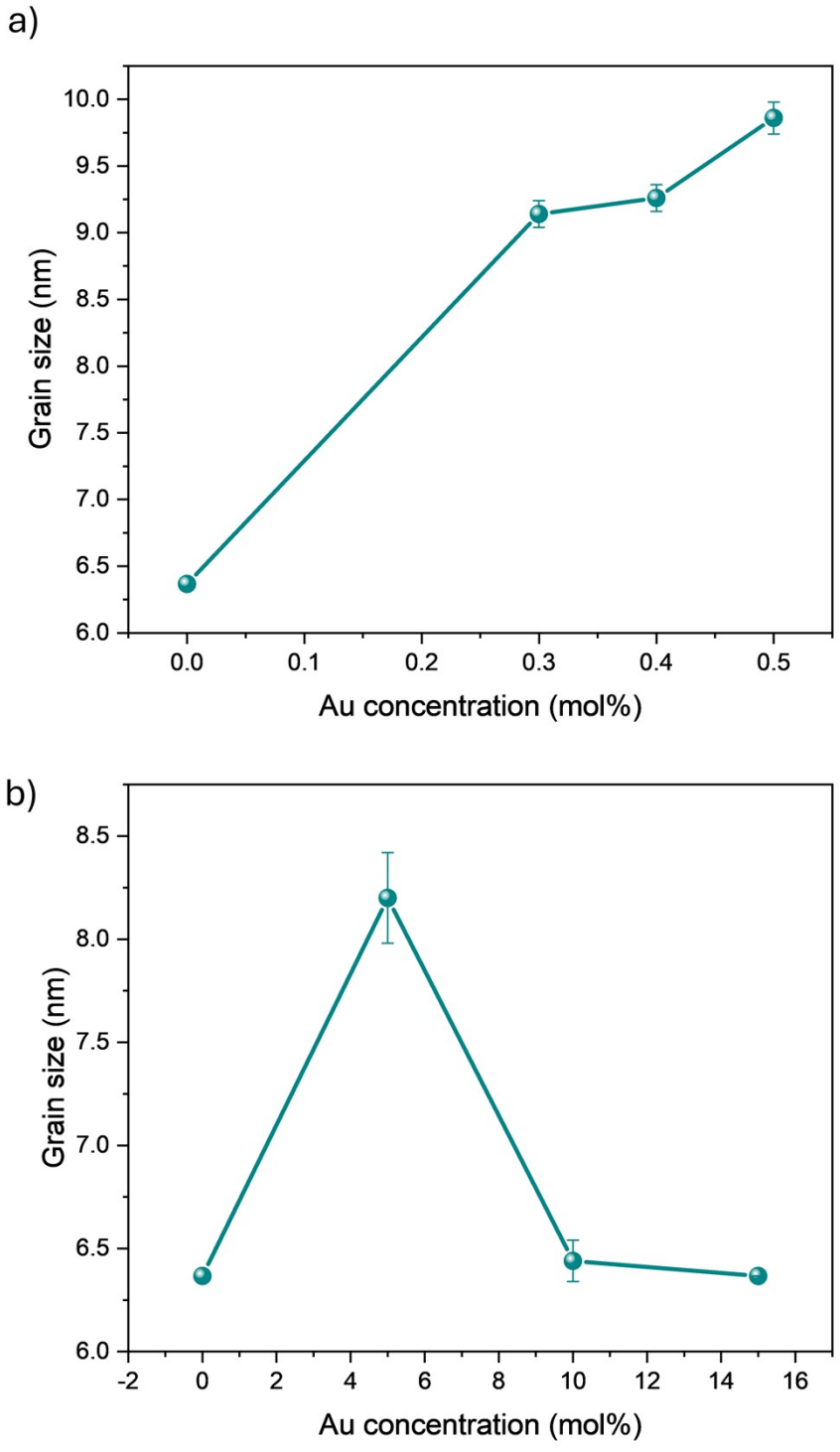

Figure S6. X-ray diffraction determination of the grain size as a function of gold concentration for (a) Low Au concentration and (b) high Au concentration regimes.

Table S1. Chemical composition of the samples determined by Rietveld refinement of the XRD results.

Au concentration (mol %)	Ce (wt -%)	O (wt -%)	Au (wt -%)
0	18.59	81.41	0
0.3	18.55	81.22	0.23
0.4	18.55	81.25	0.20
0.5	18.48	80.94	0.58
5%	17.93	78.51	3.56
10%	17.08	74.80	8.12
15%	16.95	74.21	8.84

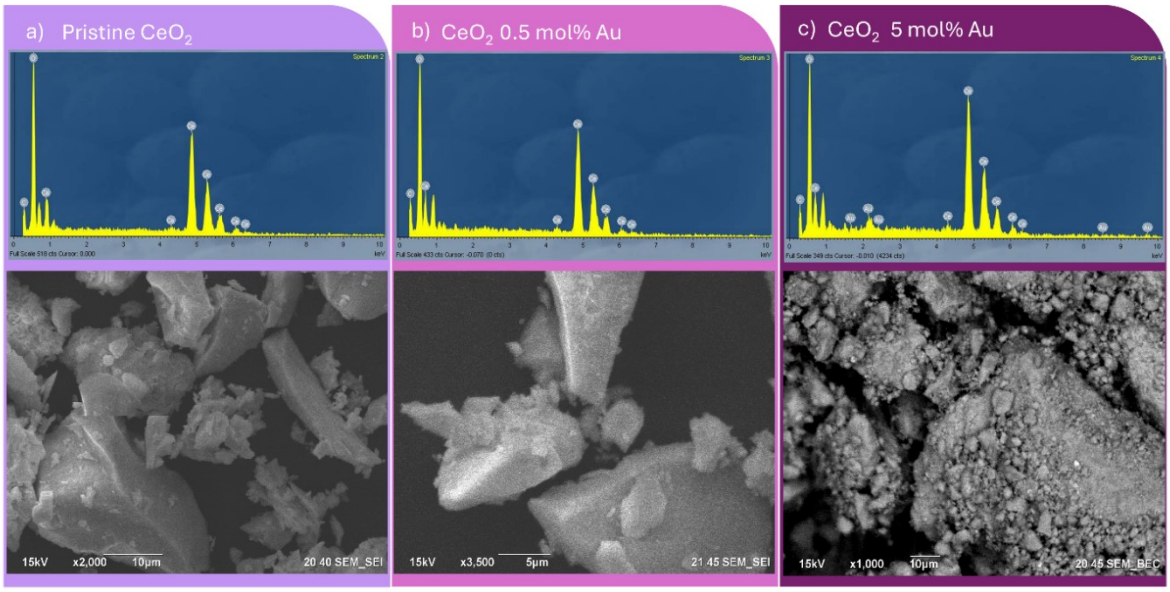

Figure S7. EDS spectra and SEM micrographs for (a) pristine CeO_2, (b) at low Au concentration regime and (c) at high concentration regime.

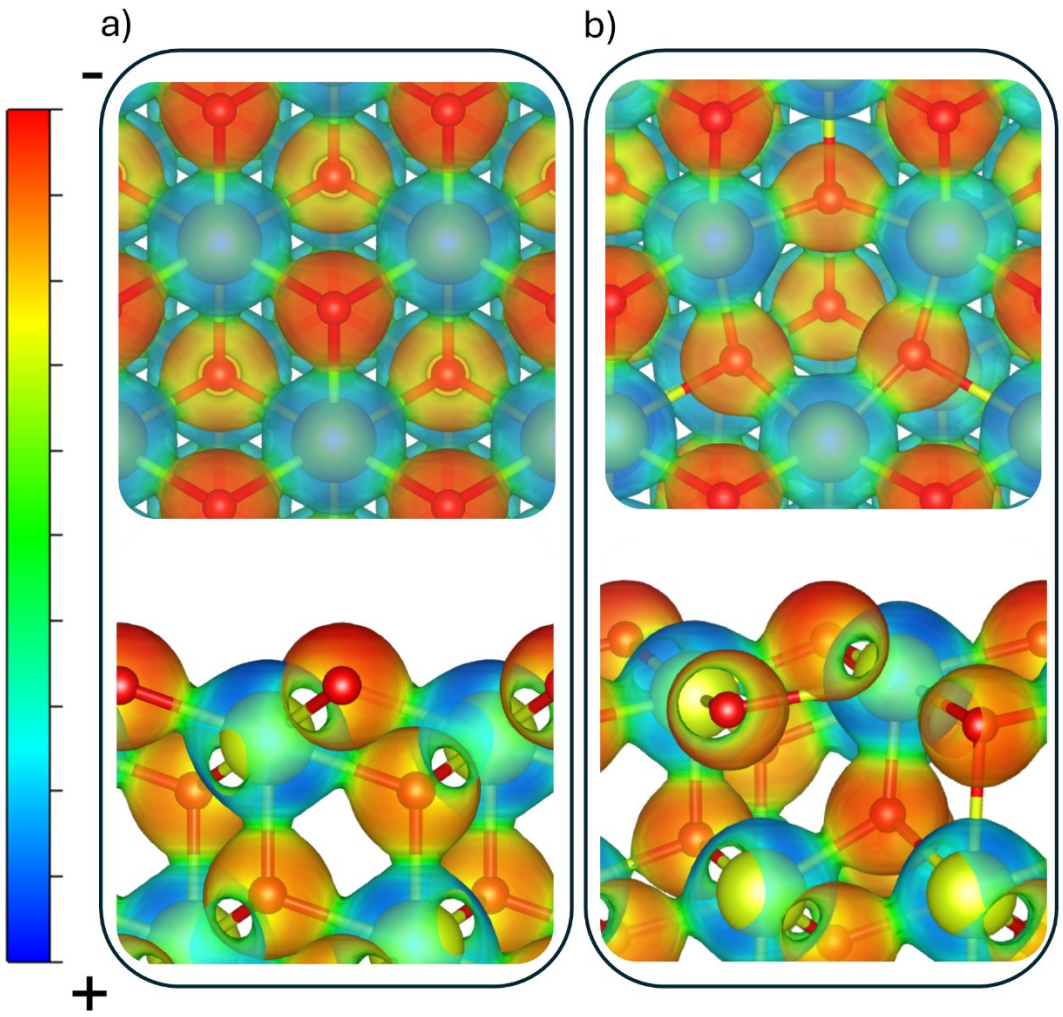

Figure S8. Electrostatic potential maps for surface models of (a) clean CeO_2 (111) and (b) surface oxygen vacancy model of CeO_2 (111).

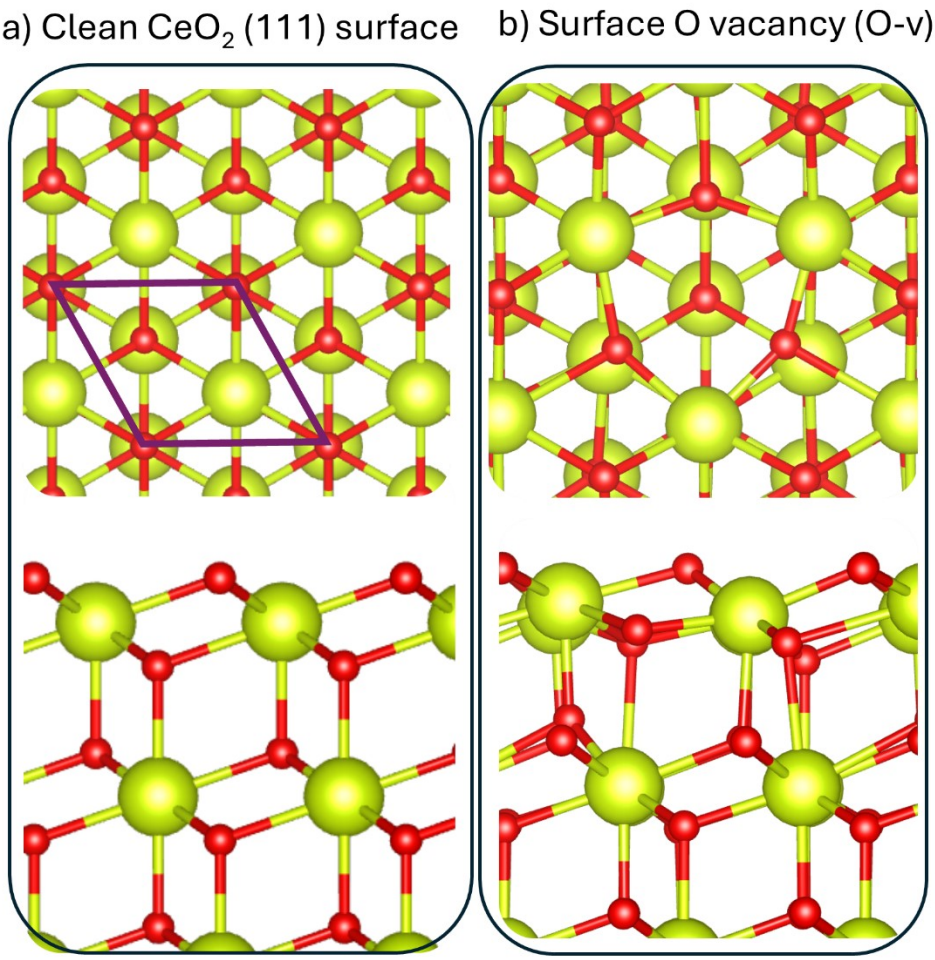

Figure S9. Surface structures for (a) clean CeO_2 (111)(b) Surface oxygen vacancy of CeO_2 (111).

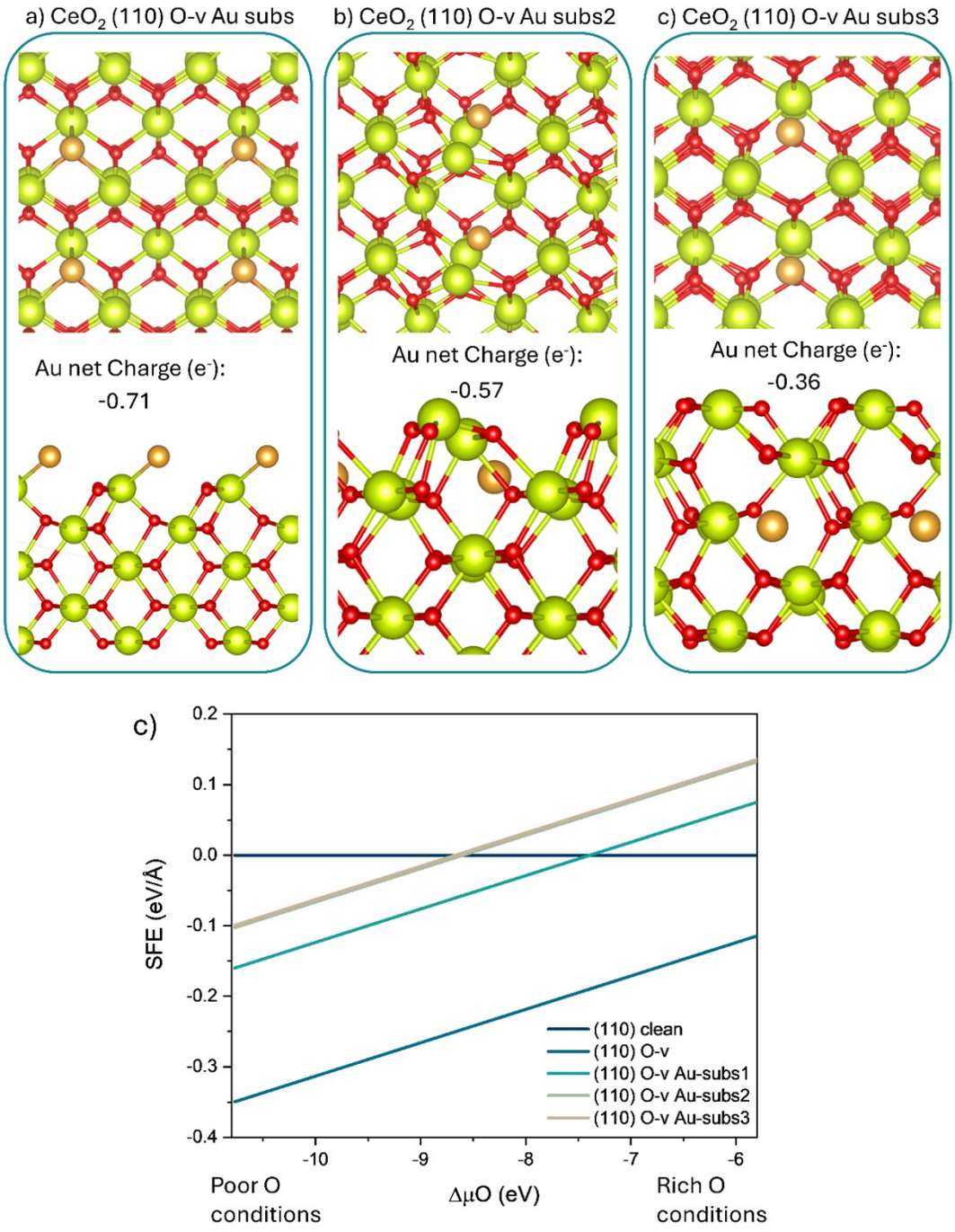

Figure S10. Adsorption of Au on CeO_2 (110) with an oxygen vacancy defect, and Bader charge analysis results. (a) substituting the nearest O to O-v (b) substituting an O below the O-v. (c) substituting an O deeper away the O-v (d) SFE as a function of chemical potential change for the above-presented models.

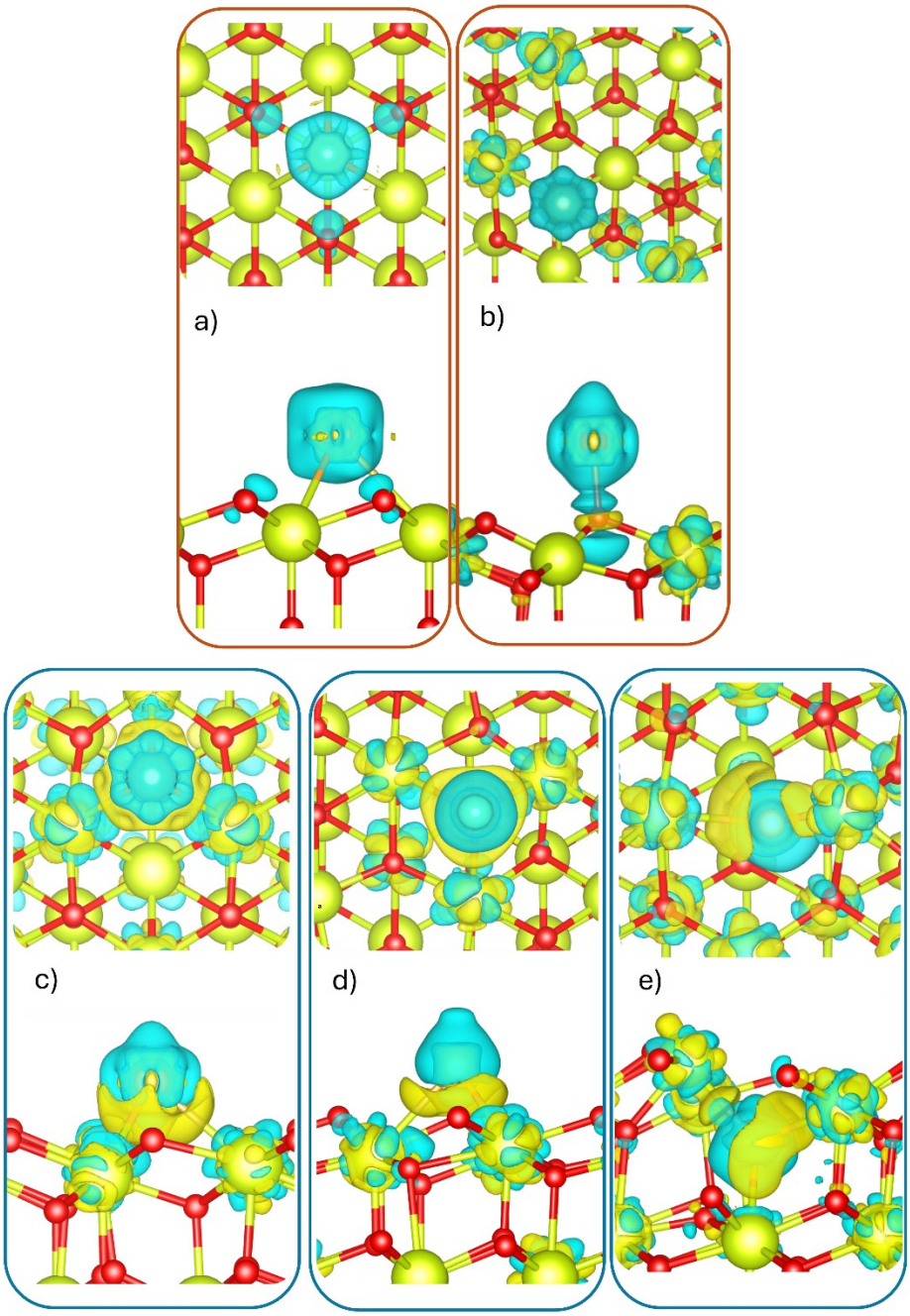

Figure S11. Charge density difference plots (isovalue = 0.006) for models of adsorption of Au on CeO_2 (111) surface with (brown frame) cationic behavior and (blue frame) anionic behavior. Blue regions depict charge density depletion, and yellow regions indicate charge density accumulation.

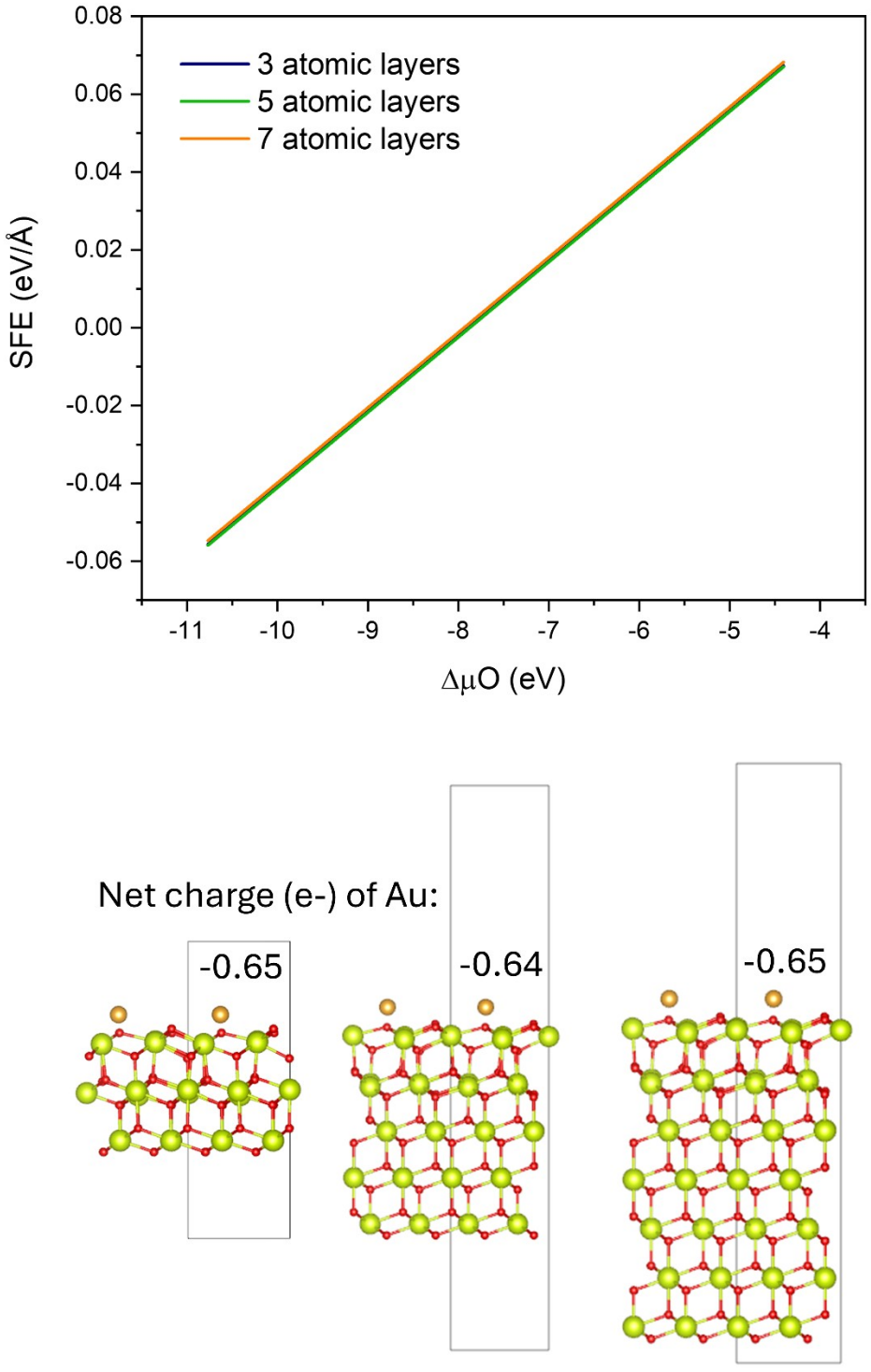

Figure S12. Surface formation energy (SFE) and Au Bader net charge comparison at increasing Ce atomic layers for the O-v O subs Au adsorption model.